Langmuir

Article

pubs.acs.org/Langmuir

Competition between Collapse and Breakup in Nanometer-Sized Thin Rings Using Molecular Dynamics and Continuum Modeling

Trung Dac Nguyen,[†] Miguel Fuentes-Cabrera,[‡] Jason D. Fowlkes,[⊥] Javier A. Diez,[§] Alejandro G. González,[§] Lou Kondic,[∥] and Philip D. Rack*[,⊥,#]

[†]National Center for Computational Sciences, Oak Ridge National Laboratory, Oak Ridge, Tennessee, United States

[‡]Computer Science and Mathematics Division and Center for Nanophase Materials Sciences, Oak Ridge National Laboratory, Tennessee, United States

[§]Instituto de Física Arroyo Seco, Universidad Nacional del Centro de la Provincia de Buenos Aires, Tandil, Argentina

[∥]Department of Mathematical Sciences, New Jersey Institute of Technology, Newark, New Jersey, United States

[⊥]Center for Nanophase Materials Sciences, Oak Ridge National Laboratory, Tennessee, United States

[#]Department of Materials Sciences and Engineering, University of Tennessee, Knoxville, Tennessee, United States

ABSTRACT: We consider nanometer-sized fluid annuli (rings) deposited on a solid substrate and ask whether these rings break up into droplets due to the instability of Rayleigh-Plateau-type modified by the presence of the substrate, or collapse to a central drop due to the presence of azimuthal curvature. The analysis is carried out by a combination of atomistic molecular dynamics simulations and a continuum model based on a long-wave limit of Navier–Stokes equations. We find consistent results between the two approaches, and demonstrate characteristic dimension regimes which dictate the assembly dynamics.

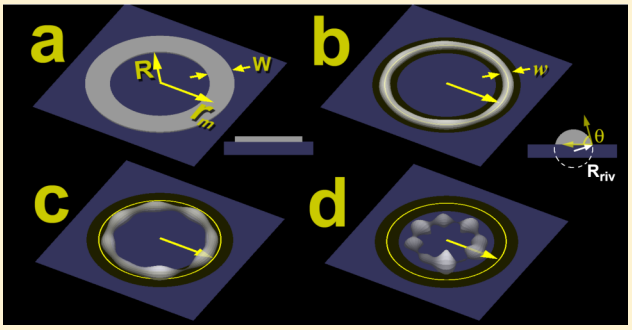

1. INTRODUCTION

Understanding competing forces in liquid phase nanostructures far from equilibrium is critical to self- and directed-assembly approaches of complex nanomaterials. Specifically, the competition between instabilities and transport is required to control the evolution of nanostructured liquids into self-organized arrays of correlated nanoparticles.[1−5] While much experimental[6−11] and computational[12−19] work has been performed historically to study the assembly of polymeric nanometric thin films, recently there has been a significant interest in studying the organization of metallic films[20−24] and lithographically patterned nanostructures.[3,4,23,25−29]

The competition between collapse and breakup for nanoscale annuli, or rings (see Figure 1) has been investigated using a continuum model (CM) based on a long-wave approximation of Navier–Stokes equations.[4,5] Large melted metal rings of 5–10 μm in radius, 100–1000 nm in width, and ∼10 nm in thickness have been studied within the framework of linear stability analysis and nonlinear continuum simulations.[5] The results revealed an interesting interplay between a Rayleigh-Plateau-like instability and thin film instability. While previous studies provide remarkable insights into the stability of larger rings, it is of particular interest to consider whether and how the continuum limit calculations could extend to the atomistic length scales. Toward this end, molecular dynamics (MD) simulation provides powerful means to capture hydrodynamic interactions from an atomistic modeling perspective, as already demonstrated in the studies on the spreading dynamics of polymer droplets,[30] the turbulent mixing between two fluids,[31] the dynamic wetting of solid–liquid interfaces,[32] and the dewetting behavior of metallic nanodroplets.[28,33]

Herein, we focus on the nonequilibrium dynamics of melted copper thin rings deposited on a graphite substrate using MD simulation in comparison with the continuum model. In addition to an analytical model recently developed to investigate the linear stability of fluid rings on supporting homogeneous substrates,[34,35] we use a modified approach that relates atomistic interactions to a conjoining–disjoining pressure and allows a more direct comparison between MD and CM results. Our study reports a remarkable quantitative agreement between atomistic and continuum models with respect to several time-dependent key characteristics of the rings. Moreover, both models successfully capture the contact line instability that may result in either a collapse or breakup depending on the ring initial geometry. The noticeable agreement of these two distinctive approaches to this nanoscopic system suggests the applicability of either alternative to obtain predictions for similar systems. This may turn out to be extremely useful when considering large systems, characterized by a typical length scale measured in tens of

Received: July 30, 2012
Revised: September 8, 2012
Published: September 9, 2012

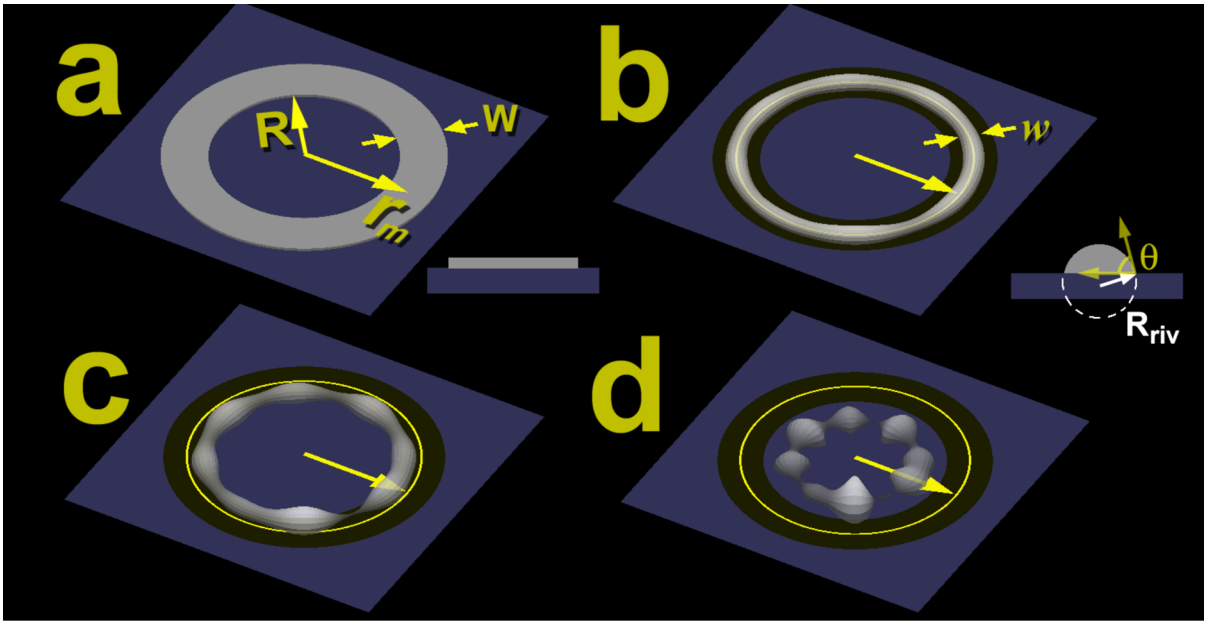

Figure 1. The thin film ring (a), characterized by an (initial) internal radius (R) and a width (W), retracts to form an annular rivulet, or ring, (b) in the liquid phase. The resulting ring has mean (time-dependent) in-plane radius r_m, contact width (w) with the underlying substrate where $w = 2R_{riv}$ sin (θ); R_{riv} is the radius of the rivulet and θ is the wetting angle of the rivulet with respect to the substrate. Ring contraction (as shown schematically in (c) and (d)) is observed for the case of a relatively large value of the aspect ratio $\psi = w/r_m$ where the rivulet contraction is driven by a large value of in-plane curvature ($\kappa' = 1/r_m$) coupled with an increasing rivulet width, w. The superimposed (yellow) circumference indicates the initial mean radius $r_m(t = 0)$ of the thin film ring while the dark ring superimposed on (b–d) indicates the original contact area of the thin film annulus with the substrate. These features are added to the schematic in order to emphasize the radial rivulet contraction over time (b → d).

nanometers, where molecular dynamics simulations become computationally expensive.

2. METHODS

2.1. Atomistic Modeling. The atomistic MD simulations are carried out using the technique employed in our previous studies.[28,33] In particular, we use three potentials to account for all of the atomic interactions: the Cu–Cu interactions are described using the embedded atom model (EAM) potential,[36] while for the C–C interactions we use an adaptive intermolecular reactive empirical bond order (AIREBO)[37] potential. The Cu–C interactions are treated with the Lennard–Jones 12–6 energy potential

$$U(\hat{r}) = \begin{cases} 4\varepsilon\left[\left(\frac{\sigma}{\hat{r}}\right)^{12} - \left(\frac{\sigma}{\hat{r}}\right)^{6}\right] & \hat{r} < \hat{r}_c \\ 0 & \hat{r} \geq \hat{r}_c \end{cases} \quad (1)$$

where ε is the depth of the potential, σ is the atomic radius, and $\hat{r}$ is the distance between the atoms. This potential is truncated and shifted to zero at a cutoff distance of $\hat{r}_c = 11$ Å for computational efficiency while ensuring energy conservation.[38]

As in a previous paper,[33] we fit the LJ potential so as to reproduce the equilibrium contact angle of liquid Cu on graphite[39] and the ab initio binding energy and distance of the Cu(111)/graphene interface.[40,41] The potential that more accurately reproduces these values has $\varepsilon = 0.01$ eV and $\sigma = 3.225$ Å. We also varied ε while keeping σ constant in order to assess how a change in the strength of the Cu–C interaction affected the dewetting behavior.[28] In particular, two other values for ε were considered, 0.02 and 0.03 eV. The latter led to a contact angle of 75.6°, which is different from the experimental equilibrium contact angle (~140°), and a binding energy about 7.5 times larger than the ab initio value. However, in the present work our selection of $\varepsilon = 0.03$ eV allows a comparison of MD results with continuum simulations which, in turn, invoke the long-wave approximation and are limited to small contact angles.

As in related studies,[28,33] a bulk liquid Cu and a graphitic substrate made of 3 layers are equilibrated at a temperature $T = 1500$ K (only the upper layer of the substrate is kept at constant temperature; the other two layers are frozen). From the bulk liquid sample, we extract rings with different width (W), inner radius (R), and thickness (H), which are then deposited on top of the graphitic substrate. Subsequently, the copper atoms are relaxed in the NVE ensemble, i.e., the number of atoms, volume, and energy are kept constant, to observe the dewetting behavior of the rings. Depending on the ring dimensions, the number of atoms in a ring varies in the range of 10^3–10^5, which together with the graphitic substrate gives a total number of atoms between 10^5 and 10^6. All simulations are carried out with the software LAMMPS.[42]

2.2. Continuum Modeling (CM). For simplicity, we consider a long-wave approach which reduces the formulation to a nonlinear fourth order partial differential equation of diffusion type. We include slip effects at the metal/substrate interface, since they are clearly present in the MD simulations, as discussed later in the text. The comparison itself with MD results is carried out by two related but slightly different approaches. The first approach is based on the linear stability analysis (LSA) of a (static) ring solution. The second approach is based on fully nonlinear time dependent simulations implementing a model which, in addition to slip, includes disjoining pressure effects. This approach allows us to consider nonlinear dynamics without including additional parameters, since the quantities entering the disjoining pressure model are directly related to the ones used in the MD simulations, as described briefly below.

2.2.1. Slip Model and Linear Stability Analysis. Long-wave theory leads to the following equation[43,44] for the film thickness $h(x,y,t)$

$$3\mu\frac{\partial h}{\partial t} + \gamma\nabla\cdot\left[h^2(h + 3l)\nabla\nabla^2 h\right] = 0 \quad (2)$$

where t is the time, (x,y) are the in-plane coordinates, μ is the fluid viscosity, and γ is the liquid–solid surface tension. Slip is included via a Navier boundary condition at the fluid–solid interface $z = 0$, i.e.:

dx.doi.org/10.1021/la303093f | Langmuir 2012, 28, 13960–13967

$$v_{x,y}(x, y, z = 0) = l\frac{\partial v_{x,y}}{\partial z} \tag{3}$$

where $v_{x,y}$ are the x and y components of the fluid velocity, the coordinate z is normal to the plane, and l is a prescribed slip length.

The linear stability analysis (LSA) of a static ring[35] is performed by studying the evolution of the perturbed static solution, h_0. In polar coordinates, we have the following:

$$h(r, \varphi, t) = h_0(r, \varphi) + \varepsilon h_1(r, \varphi, t) \tag{4}$$

where ε is the (small) amplitude of the perturbation specified as a normal mode:

$$h_1(r, \varphi, t) = \hat{h}_1(r)\cos(n\varphi)\exp(\omega(n)t) \tag{5}$$

with $\omega(n)$ being the growth rate of the n-th mode. Plugging eq 4 into the governing eq 2 and linearizing in terms of h_1 lead to an eigenvalue problem which is solved by a pseudospectral method.[35] The resulting eigenvalues, $\omega(n)$, are determined as a function of the aspect ratio of the ring, $\psi = w/r_m$, where w are r_m are its width and the mean radius, both time dependent.

2.2.2. Disjoining Pressure Model: Numerical Simulations. We proceed to develop a nonlinear CM to capture the time evolution of the rings. Here, the disjoining pressure is included to model the long-range intermolecular interaction between the liquid and the substrate. Since this interaction is considered in the MD simulations through the LJ 12−6 potential, we introduce this effect by integrating this interaction over an infinitely extended substrate and on a liquid column of height h and unit cross sectional area.[45,46]

According to the atomistic model used in eq 1, the resultant interaction energy of a single particle in the liquid with all of the particles in the substrate can be written as follows:

$$V = \int_{V_S} Un_s \, dV \tag{6}$$

where V_S is the substrate volume, and n_s is the number of particles per unit volume in the substrate. If we consider all of the liquid particles within a column of height h and unit area, then we obtain the energy per unit area in the van der Waals form as follows:[45]

$$V_{vdW}(h) = \int_{z=h}^{z=c\sigma} Vn_l \, dz = \int_{z=h}^{z=c\sigma}\int_{V_S} n_s n_l U \, dV \, dz \tag{7}$$

where n_l is the number of liquid particles per unit volume, and $c\sigma$ is the distance of closest approach of molecules of the liquid and the solid, with c a constant of order of unity. By plugging eq 1 into eq 7, and performing the integration, we have

$$V_{vdW}(h) = \pi n_l n_s \varepsilon\left(\frac{\sigma^{12}}{90h^8} - \frac{\sigma^6}{3h^2}\right) + V_0 \tag{8}$$

where the constant V_0 is given by

$$V_0 = \pi n_l n_s \varepsilon\sigma^4\left(\frac{1}{3c^2} - \frac{1}{90c^8}\right) \tag{9}$$

such that $V_{vdW} = 0$ at $h = c\sigma$, and $V_{vdW} \to V_0$ for $h \to \infty$. Taking the first derivative of this energy potential, we obtain the disjoining pressure as follows:

$$\begin{aligned}\Pi(h) &= -\frac{dV_{vdW}}{dh} \\ &= 2\pi n_l n_s \varepsilon\left(\frac{2\sigma^{12}}{45h^9} - \frac{\sigma^6}{3h^3}\right) \\ &= \kappa\left[\left(\frac{h_*}{h}\right)^9 - \left(\frac{h_*}{h}\right)^3\right]\end{aligned} \tag{10}$$

where

$$h_* = \left(\frac{2}{15}\right)^{1/6}\sigma = 0.715\sigma \tag{11}$$

is the thickness at which $\Pi(h_*) = 0$, and

$$\kappa = \sqrt{\frac{10}{3}}\pi n_l n_s \varepsilon\sigma^3 \tag{12}$$

The static contact angle, θ, can now be obtained from the Young−Laplace condition:

$$\cos\theta = 1 - \frac{S}{\gamma} = 1 - \frac{4 - 120c^6 + 4560^{1/3}c^8}{360\gamma c^8}\pi n_l n_s \varepsilon\sigma^4 \tag{13}$$

where $S = -V_{vdW}(h_*)$ is the spreading parameter. Thus, for given material parameters, eq 13 allows to obtain the corresponding value of c.

To directly compare CM simulations with the MD results, we use the following parameters: copper density ρ_l = 8.0 g/cm^3, carbon density ρ_s = 3.23 g/cm^3, σ = 3.225 Å, ε = 0.03 eV, and γ = 1.304 N/m. The particle densities are obtained as $n_l = \rho_l N_a/M_l$ and $n_s = \rho_s N_a/M_s$, where N_a is the Avogadro number, and M_l = 63.536 g/mol and M_s = 12.01 g/mol are the copper and carbon atomic weights, respectively. For this set of parameters, and considering that MD simulations yield[28] θ = 75.6°, we have c = 0.55.

We will report here numerical results obtained by solving eq 2 with the addition of the disjoining pressure term:

$$\nabla\cdot[h^2(h + 3l)\nabla\Pi] \tag{14}$$

where Π is given by eq 10. We employ a procedure based on the alternating direction implicit (ADI) method which is described in detail elsewhere.[47] We note that there is only one free parameter left to proceed to a comparison with MD results, that is, the slip length, l. The remaining parameter is copper viscosity, which we take as μ = 4.38 mPa s.

3. RESULTS

The simulated system is depicted in Figure 1 in which a fluid thin ring is deposited on a solid graphite substrate. We choose an initial rectangular cross-section geometry to be consistent with our previous work, which mimics experimental geometries of lithographically patterned solid nanostructures that are irradiated with a nanosecond pulsed laser which rapidly melts the far-from-equilibrium structures and allows them to evolve.[27] The nanometer-sized rings have smaller (initial) radius and width than, yet similar thickness to, those in experiment: inner radius (R) in the range of 160−320 Å, width (W) 10−80 Å, and thickness (H) 10−50 Å. The number of atoms simulated varies in the range of 10^5−10^6.

3.1. Connection between CM and MD Simulations.

One of the key factors that governs the dynamics of fluid thin films is the boundary condition at the solid−fluid interface.[48−50] Continuum simulations can be performed within a no-slip regime, as often done in previous works.[2−5] Similar simulations,[28] however, suggested that the slip length could be as large as some tens of Angstroms. As will be shown later by MD velocity profiles, slip is indeed present in this system. It is nevertheless difficult to extract accurately the slip length, l, from the MD simulations in the presence of thermal noise and fast dynamics. We instead carry out CM simulations using the disjoining pressure and slip model to determine the slip length with which the rings entirely collapse after the same duration as in MD simulations. For this purpose, we assume that the rings have azimuthal symmetry and their thickness is dependent only upon the radial distance, i.e., $h = h(r)$. An example of the profile evolution in this type of simulations is shown in Figure 2. The

dx.doi.org/10.1021/la303093f | Langmuir 2012, 28, 13960−13967

cross section of the initial condition used for all reported simulation is a rectangle.

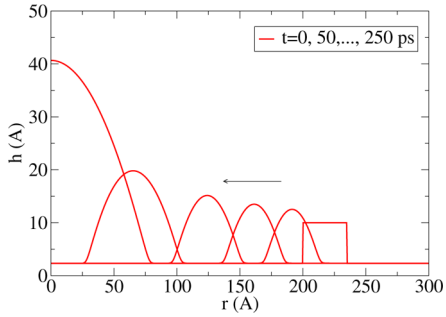

Figure 2. Time evolution of the thickness profile in an azimuthally symmetric CM simulation, showing the collapse of the ring into a single central drop. Initially, the ring dimensions are R = 200 Å, W = 35 Å, H = 10 Å, and the cross section is a rectangle, as described in the text. The slip length is taken as l = 70 Å. The arrow points the direction of increasing time.

Figure 3(a) shows that this collapse time in the continuum simulations indeed strongly depends on l; the greater the slip

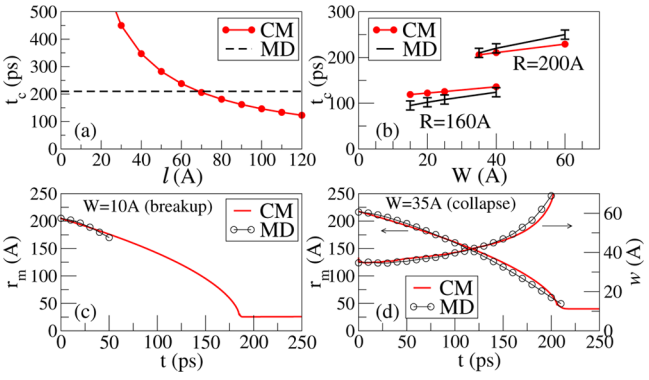

Figure 3. (a) Collapse times, t_c, obtained using CM simulations versus slip length, illustrating the optimum value for l = 70 Å. (b) Collapse times for R = 160 Å and 200 Å with different ring widths obtained by MD versus continuum simulations with l = 70 Å. (c) Comparison of the mean radius $r_m(t)$ for a ring with R = 200 Å, W = 10 Å, and H = 10 Å up to the breakup time of about 50 ps in the MD simulations. (d) Comparison of both $r_m(t)$ and width $w(t)$ with R = 200 Å, W = 35 Å, and H = 10 Å until collapse onto a single central drop.

length, the faster the ring collapses. For the particular choice of the initial conditions considered, we find that a good agreement of collapse time is obtained for l = 70 Å. To confirm that the MD and continuum simulations lead to consistent predictions for collapse times as the initial conditions are varied, we fix this value of l and compare directly the collapse times for different values of R and W (see Figure 3(b)). Remarkably, the time evolution of the mean radius $r_m(t)$ predicted by the continuum model match with that in MD simulations for both rings, as shown in Figure 3(c,d). The consistency between atomistic and continuum models is maintained until the ring either breaks up for W = 10 Å, or collapses for W = 35 Å. It is therefore evident that both approaches can predict qualitatively identical evolutions of the rings as long as the azimuthal symmetry of the rings is present, i.e., breakup has not yet occurred.

3.2. Stability Analysis. Previous studies have shown that the dynamics of thin films on a solid substrate is strongly influenced by Raleigh-Plateau instability.[2,4,5,34,50] Given a fixed ring geometry and using a slip model (see Section 2.2.1) we can predict the perturbation mode with the fastest growing rate, which presumably determines the number of droplets being formed.[2,35] The dispersion curve in Figure 4 obtained from the LSA analysis shows the dependence of the fastest growing perturbation mode, n_{max}, on the (time-dependent) aspect ratio of the ring, ψ.

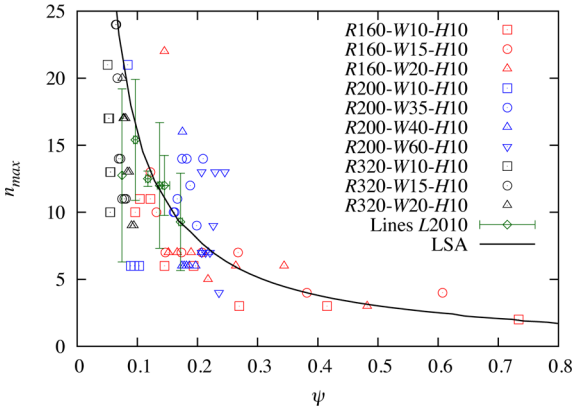

Figure 4. Mode number of the perturbation of maximum growth rate (n_{max}) as a function of the ring aspect ratio (ψ) from MD simulations (symbols). Dimensions are in Angstroms. The simulated lines with the effective aspect ratio $\psi_e = w/R_e$ where the effective radius R_e is defined as $R_e = L/2\pi$ = 320 Å are also included. The error bars at the data points of the lines are obtained by averaging n_{max} within each window of $[\psi_e; \psi_e + \Delta\psi]$ where $\Delta\psi$ = 0.01. For a given ring (and line) geometry, the data points correspond to different times during the course of the simulation. The solid line is obtained using the LSA of the continuum model.

To extract the fastest growing perturbation mode from the MD simulations, we perform Fourier transforms of the ring width along its circumference during the collapse process or before the first breakup event occurs. We use this procedure because once the rings break up, the geometry of individual segments is completely different from the slightly perturbed ring used to analyze the instability with the slip model, making the comparison less meaningful. We choose the ring width instead of thickness as the later quantity is closer to the atomic length scale and hence is more sensitive to thermal noise. From the Fourier spectrum of the ring width at a given time, we identify the location of the highest peak, which indicates the most dominant spatial frequency, f_{max}, of the fluctuating width. The corresponding mode number, $n_{max} = 2\pi f_{max}$, is then attributed to the fastest growing perturbation mode to be compared against the LSA.

We carry out MD simulations of rings with the same initial thickness (H = 10 Å) but with different initial inner radii (R = 160 Å, 200 Å, and 320 Å) and widths (W = 10 Å, 15 Å, and 20 Å). During collapse, the mean radius, r_m, decreases while the average width, w, increases due to mass conservation. Consequently, ψ increases over time, which according to the LSA corresponds to a decrease in n_{max}. As shown in Figure 4, this expected feature is observed in MD simulations for all studied cases, particularly for the rings that entirely collapse, for example, with R = 160 Å.

We have also performed MD simulations of straight lines with the length of L = 2010 Å, which is equal to the inner perimeter of the rings with R = 320 Å, while varying the width

dx.doi.org/10.1021/la303093f | Langmuir 2012, 28, 13960−13967

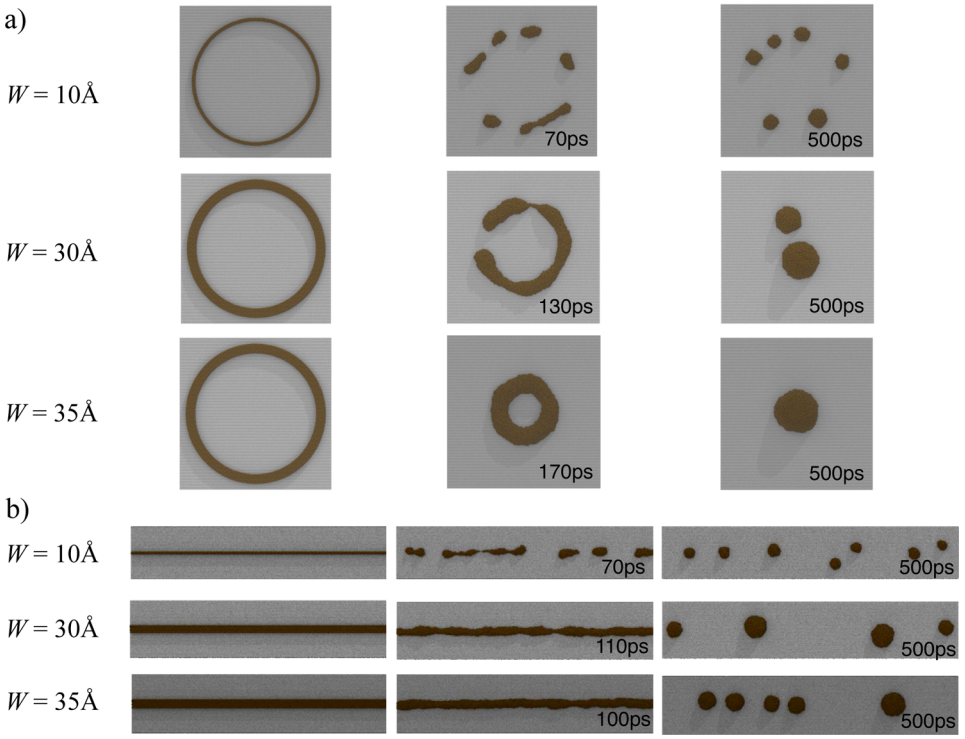

Figure 5. Time evolution of (a) rings of R = 200 Å and (b) lines of L = 1200 Å with H = 10 Å and different initial widths. Initial configurations are shown in the left columns.

W = 20−60 Å and thickness H = 10−30 Å, to investigate how the initial geometry influences the fastest growing modes. Periodic boundary conditions are applied at the ends of the lines to eliminate edge contraction effects at the early stage. Fourier analysis of the line width profile is performed in a similar manner to the ring width to investigate the evolution of the perturbations. Our analysis reveals that the fastest growing perturbation modes of the lines are consistent with that of the rings and with the dispersion curve predicted by the LSA for small aspect ratio, ψ.

3.3. Assembly Dynamics. Having shown that the initial ring dimensions play an important role in determining the fastest growth mode, we proceed to correlate the initial geometry to the resultant self-organized droplet array. We have also demonstrated in Section 3.1 that MD simulations can produce consistent results with the CM in the early stage at a certain slip length. Now we proceed to examine whether the current atomistic model could capture the dynamics of the rings in the late stage, i.e., after the first breakup event.

Figure 5(a) shows a representative time evolution of rings of different widths, but with the same initial inner radius R = 200 Å, and thickness H = 10 Å. The first column illustrates the initial geometry and the middle and far right column show the ring at approximately 100 and 500 ps, respectively. We have also studied lines with equivalent length ($2\pi R$), thickness and width, so as to elucidate, by comparisons with the rings, the forces operative in the competition between the collapse and breakup process (Figure 5(b)).

The assembly dynamics have different stages involved in the evolution of the initial rectangular cross-section rings to the subsequent nanoparticle array. Initially, the rectangular cross-section quickly minimizes its surface energy (∼10 ps) by transforming into circular cross-section whose contact width (w) and contact angle (θ) are governed by Young−Laplace condition (see Figure 1). The subsequent breakup time depends on the width of the ring/rivulet that forms on the substrate. For the narrowest ring (w = 10 Å), the equilibrated initial radius is the smallest one (w = 9.6 Å), and thus it has the shortest droplet formation time (∼40 ps), which is approximately the time for an equivalent line to break up (∼40 ps). For the W = 30 Å ring (Figure 5(a)), the equilibrated initial rivulet width is larger (w = 18.6 Å), and the breakup time is longer, ∼120 ps (the mean ring radius, r_m, at breakup is 142 Å compared with 215 Å at t = 0, due to the contraction that occurs prior to breakup). The equivalent line for this width has a breakup time of ∼130 ps. Thus, the wider ring has a longer breakup time and therefore it contracts further before breakup.

Interestingly, the ring structures have equivalent or earlier breakup times than the corresponding straight lines, which is counterintuitive since the radial collapse tends to increase the ring width. We hypothesize that in advanced stages, the collapse and breakup modes have grown enough to allow for nonlinear interaction which transfers energy from the long wave mode (collapse) to the short wave one (breakup). Unlike in the straight rivulet, this effect accelerates the breakup process. Finally, if one compares the straight line and ring for W = 35 Å, the line breaks up at ∼210 ps and forms 5 droplets (Figure 5(b)); however this time scale is prohibitively long as the azimuthal curvature driven collapse dominates and a single central droplet is formed for this ring (∼210 ps).

Before we leave the discussion of the collapse versus breakup, it is relevant to mention that the final number of drops in the MD simulations is ultimately smaller than the number of perturbation modes on the ring or line prior to initial pinch-off of the fastest growing mode. Similar coarsening effect observed in the final droplet size as described previously[5] is due to circumferential transport after breakup. This is apparent by the intermediate and final snapshots of the W = 30 Å ring and most

dx.doi.org/10.1021/la303093f | Langmuir 2012, 28, 13960−13967

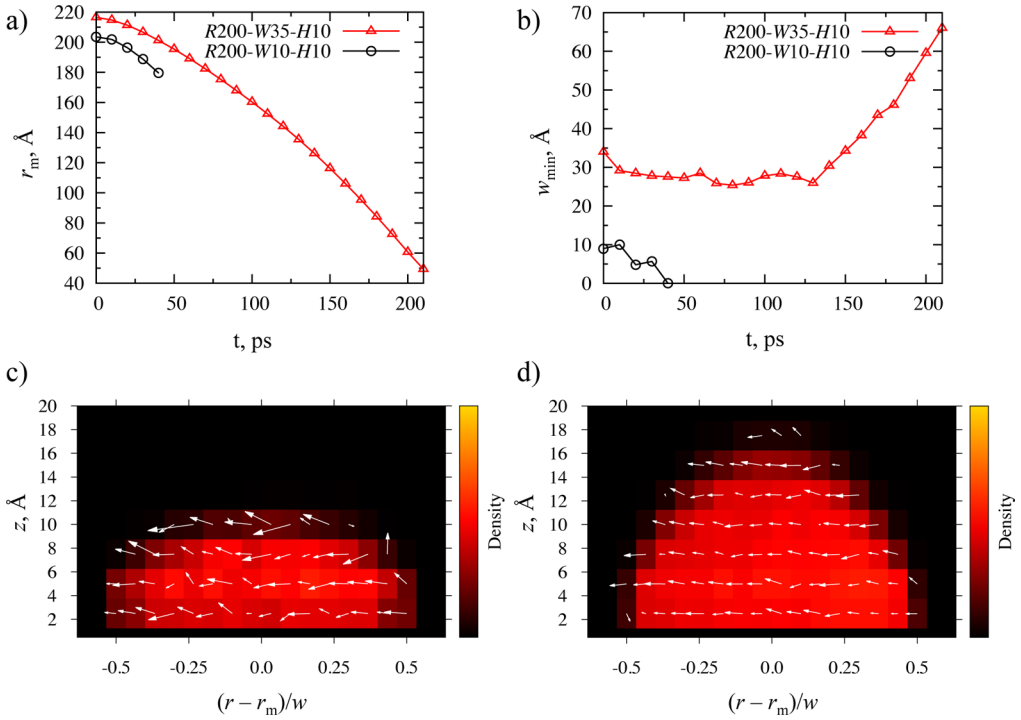

Figure 6. Time evolution of (a) the mean radius (r_m) and (b) the minimum ring width (w_{min}) for R = 200 Å, W = 10 Å, H = 10 Å (breakup), and R = 200 Å, W = 35 Å, H = 10 Å (collapse) (see Figure 5). Atom velocity profile and density of (c) R = 200 Å, W = 10 Å, H = 10 Å at 4 0 ps, and (d) R = 200 Å, W = 35 Å, H = 10 Å (bottom) at 40 ps. The color map represents the atom density. The radial velocities point toward the ring center (not shown). In (c,d), w is the average width of the ring along its circumference.

of the lines. For instance, if one estimates the number of perturbation minima in the W = 30 Å ring at 130 ps (Figure 5(a)), one expects approximately 7 droplets to form. However, the circumferential transport after breakup competes with the growing instability and in this case results in only 2 droplets.

The breakup-collapse transition also occurs as we vary the initial thickness of the rings. We observe that rings with R = 160 Å always collapse as their thickness is varied in the range of H = 10−30 Å. On the other hand, for larger inner radius, R = 320 Å, the ring with H = 30 Å collapses, while for H = 10 Å and 20 Å they break up into 6 and 2 droplets, respectively. For fixed values of R and W, the thicker the rings, the more likely they collapse. Thus, the initial thickness is another useful parameter for controlling the number and size of stable droplets formed by the ring instability.

To further characterize the difference between the rings that collapse and those that break up into droplets, we measure the variation in the ring mean radius (r_m) and minimum width (w_{min}) over time, where w_{min} = 0 reveals the breakup time. Figure 6 demonstrates the analysis for R = 200 Å, H = 10 Å, with W = 10 Å and 35 Å; the former breaks up while the latter collapses (see Figure 5(a)). At t = 40 ps, as w_{min} reaches zero, the W = 10 Å ring broke. For W = 35 Å, the radius continually contracts with increasing velocity while the width initially slightly decreases due to a reaccommodation process, and later on remains approximately constant up to 125 ps. Eventually, at this time, the radial contraction rate is such that it dominates the breakup growth rate and, consequently, due to the fact that the volume is conserved, the contact width increases as r_m decreases, thus leading to collapse at 210 ps. It is therefore demonstrated that the capillary pressure collapse suppresses the breakup for the wider ring, leading to a complete collapse; whereas, the narrower ring breaks up as the perturbation growth outpaces the radial contraction velocity.

The average radial velocity profiles of the atoms across the cross-section for these two rings at 40 ps are shown in Figure 6(c,d). These figures indicate that both rings are accelerating toward the center, and that the narrower ring has slightly higher velocity. For the narrower ring, the atom velocities are more randomly distributed across the ring cross section, which we attribute to the evolving Rayleigh-Plateau instability; namely at the localized perturbation peaks and troughs, material transport away from the trough and toward the peaks[5] contribute to the more randomized (albeit greater) velocities. There could also be contributions from the smaller sampling set for the smaller rings as well as interfacial effects at the Cu−C boundary. Meanwhile, for the wider ring, the radial velocities appear more correlated and align toward the center of the ring until the ring entirely collapses. We note that from the nonzero velocity of the atoms in contact with the substrate in both cases, it is reasonable to assume a considerable slip length in these systems.[28]

4. CONCLUSIONS

Atomistic (MD) and continuum models (CM) are shown to yield remarkably consistent predictions on the breakup and collapse of nanometer-sized liquid copper rings on graphite. The atomistic simulations use the Lennard−Jones 12−6 potential to describe the liquid copper−graphite interactions, while in the continuum modeling we directly convert this potential to a disjoining pressure. Furthermore, once we estimate an appropriate slip-length for the continuum simulations, the quantitative dynamics of the two methods are also in very good agreement for the collapse and the initial stages of the instability. Strong nonlinear effects present in MD

dx.doi.org/10.1021/la303093f | *Langmuir* 2012, 28, 13960−13967

simulations are related to circumferential transport, but the general trend for the number of drops in the early breakup, specially for thin rings, as well as characteristics of collapse are consistent with continuum models predictions. Importantly, this agreement between the two approaches inspires the possibility for multiple length scale simulations of nano-to-mesoscale self-assembly.

AUTHOR INFORMATION

Corresponding Author

*E-mail: prack@utk.edu.

Notes

The authors declare no competing financial interest.

ACKNOWLEDGMENTS

T.D.N. acknowledges the support from the Office of Science of the U.S. Department of Energy under Contract No. DE-AC05-00OR22725. This research used resources of the Oak Ridge Leadership Computing Facility at the Oak Ridge National Laboratory, which is supported by the Office of Science of the U.S. Department of Energy under Contract No. DE-AC05-00OR22725. J.F., M.F.C., and P.R. acknowledge support from the U.S. Department of Energy, Basic Energy Sciences, Materials Sciences and Engineering Division for supporting the molecular dynamics simulations and understanding the fundamental mechanisms operative during liquid phase, thin film assembly. L.K. acknowledges support by the NSF Grant No. DMS-0908158. J.A.D. and A.G.G. acknowledge CONICET-Argentina for travel support within the International Cooperation Program and ANPCyT-Argentina for support within the project PICT 2498/06.

REFERENCES

(1) González, A. G.; Diez, J. A.; Gratton, R.; Gomba, J. Rupture of a fluid strip under partial wetting conditions. *Europhys. Lett.* **2007**, *77*, 440011−440015.

(2) Diez, J. A.; González, A. G.; Kondic, L. On the breakup of fluid rivulets. *Phys. Fluids* **2009**, *21*, 082105.

(3) Kondic, L.; Diez, J. A.; Rack, P. D.; Guan, Y.; Fowlkes, J. D. Nanoparticle assembly via the dewetting of patterned thin metal lines: Understanding the instability mechanisms. *Phys. Rev. E* **2009**, *79*, 026302.

(4) Wu, Y.; Fowlkes, J. D.; Rack, P. D.; Diez, J. A.; Kondic, L. On the breakup of patterned nanoscale copper rings into droplets via pulsed-laser-induced dewetting: competing liquidphase instability and transport mechanisms. *Langmuir* **2010**, *26*, 11972−11979.

(5) Wu, Y.; Fowlkes, J. D.; Roberts, N. A.; Diez, J. A.; Kondic, L.; González, A. G.; Rack, P. D. Competing liquid phase instabilities during pulsed laser induced self-assembly of copper rings into ordered nanoparticle arrays on SiO2. *Langmuir* **2011**, *27*, 13314−13323.

(6) Brochard-Wyart, F.; de Gennes, P. Dynamics of partial wetting. *Adv. Colloid Interface Sci.* **1992**, *39*, 1−11.

(7) Reiter, G. Dewetting of thin polymer-films. *Phys. Rev. Lett.* **1992**, *68*, 75−78.

(8) Sharma, A.; Reiter, G. Instability of thin polymer films on coated substrates: Rupture, dewetting, and drop formation. *J. Colloid Interface Sci.* **1996**, *178*, 383−399.

(9) Seemann, R.; Herminghaus, S.; Jacobs, K. Dewetting patterns and molecular forces: A reconciliation. *Phys. Rev. Lett.* **2001**, *86*, 5534−5537.

(10) Du, B.; Xie, F.; Wang, Y.; Yang, Z.; Tsui, O. K. C. Dewetting of polymer films with built-in topographical defects. *Langmuir* **2002**, *18*, 8510−8517.

(11) Neto, C.; Jacobs, K. Dynamics of hole growth in dewetting polystyrene films. *Phys. A* **2004**, *339*, 66−71.

(12) Huh, C.; Scriven, L. E. Hydrodynamic model of steady movement of a solid/liquid/fluid contact line. *J. Colloid Interface Sci.* **1971**, *35*, 85−101.

(13) Coninck, J. D.; Hoorelbeke, S.; Valignat, M. P.; Cazabat, A. M. Effective microscopic model for the dynamics of spreading. *Phys. Rev. E* **1993**, *48*, 4549−4555.

(14) Milchev, A.; Binder, K. Dewetting of thin polymer films adsorbed on solid substrates: A Monte Carlo simulation of the early stages. *J. Chem. Phys.* **1997**, *106*, 1978.

(15) Schwartz, L. W.; Roy, R. V.; Eley, R. R.; Petrash, S. Dewetting patterns in a drying liquid film. *J. Colloid Interface Sci.* **2001**, *234*, 363−374.

(16) Becker, J.; Grün, G.; Seemann, R.; Mantz, H.; Jacobs, K.; Mecke, K. R.; Blossey, R. Complex dewetting scenarios captured by thin-film models. *Nat. Mater.* **2003**, *2*, 59−63.

(17) Fetzer, R.; Jacobs, K.; Münch, A.; Wagner, B.; Witelski, T. P. New slip regimes and the shape of dewetting thin liquid films. *Phys. Rev. Lett.* **2005**, *95*, 127801.

(18) Min, D. H.; Wong, H. Rayleigh's instability of Lennard−Jones liquid nanothreads simulated by molecular dynamics. *Phys. Fluids* **2006**, *18*, 024103.

(19) Bertrand, E.; Blake, T. D.; Ledauphin, V.; Ogonowski, G.; Coninck, J. D.; Fornasiero, D.; Ralston, J. *Langmuir* **2007**, *23*, 3774−3785.

(20) Bischof, J.; Scherer, D.; Herminghaus, S.; Leidere, P. Dewetting modes of thin metallic films: Nucleation of holes and spinodal dewetting. *Phys. Rev. Lett.* **1996**, *77*, 1536−1539.

(21) Herminghaus, S.; Jacobs, K.; Mecke, K.; Bischof, J.; Fery, A.; Ibn-Elhaj, M.; Schlagowski, S. Spinodal dewetting in liquid crystal and liquid metal films. *Science* **1998**, *282*, 916−919.

(22) Henley, S. J.; Carey, J. D.; Silva, S. R. P.Pulsed-laser-induced nanoscale island formation in thin metal-on-oxide films. *Phys. Rev. B* **2005**, *72*, 195408.

(23) Kojima, Y.; Kato, T. Nanoparticle formation in Au thin films by electron-beam-induced dewetting. *Nanotechnology* **2008**, *19*, 255605.

(24) Wu, Y.; Fowlkes, J. D.; Rack, P. D. The optical properties of Cu−Ni nanoparticles produced via pulsed laser dewetting of ultrathin films: The effect of nanoparticle size and composition on the Plasmon response. *J. Mat. Res.* **2011**, *26*, 277.

(25) Rack, P. D.; Guan, Y.; Fowlkes, J. D.; Melechko, A. V.; Simpson, M. L. Pulsed laser dewetting of patterned thin metal films: A means of directed assembly. *Appl. Phys. Lett.* **2008**, *92*, 223108.

(26) Fowlkes, J. D.; Wu, Y.; Rack, P. D. Directed assembly of bimetallic nanoparticles by pulsed laser induced dewetting: A unique time and length scale regime. *ACS Appl. Mater. Interfaces* **2010**, *2*, 2153−2161.

(27) Fowlkes, J. D.; Kondic, L.; Diez, J. A.; Wu, Y.; Rack, P. D. Self-assembly versus directed assembly of nanoparticles via pulsed laser induced dewetting of patterned metal films. *Nano Lett.* **2011**, *11*, 2478−2485.

(28) Fuentes-Cabrera, M.; Rhodes, B. H.; Fowlkes, J. D.; Lopez-Benzanilla, A.; Terrones, H.; Simpson, M. L.; Rack, P. D. Molecular dynamics study of the dewetting of copper on graphite and graphene: Implications for nanoscale self-assembly. *Phys. Rev. E* **2011**, *83*, 041603.

(29) Fowlkes, J. D.; Horton, S.; Fuentes-Cabrera, M.; Rack, P. D. Signatures of the rayleigh-plateau instability revealed by imposing synthetic perturbations on nanometer-sized liquid metals on substrates. *Angew. Chem., Int. Ed.* **2012**, *51*, 8768−8772.

(30) Heine, D. R.; Grest, G. S., ; Ill, E. B. W. Spreading dynamics of polymer nanodroplets in cylindrical geometries. *Phys. Rev. E* **2004**, *70*, 011606.

(31) Kadau, K.; Germann, T. C.; Hadjiconstantinou, N. G.; Lomdahl, P. S.; Dimonte, G.; Holian, B. L.; Alder, B. J. Nanohydrodynamics simulations: An atomistic view of the Rayleigh- Taylor instability. *Proc. Natl. Acad. Sci. U.S.A.* **2004**, *101*, 5851−5855.

(32) Gentner, F.; Ogonowski, G.; Coninck, J. D. Forced wetting dynamics: A molecular dynamics study. *Langmuir* **2003**, *19*, 3996−4003.

(33) Fuentes-Cabrera, M.; Rhodes, B. H.; Baskes, M. I.; Terrones, H.; Fowlkes, J. D.; Simpson, M. L.; Rack, P. D. Controlling the velocity of jumping nanodroplets via their initial shape and temperature. *ACS Nano* **2011**, *5*, 7130−7136.
(34) Wu, Y.; Fowlkes, J. D.; Rack, P. D.; Diez, J. A.; Kondic, L. On the breakup of patterned nanoscale copper rings into droplets via pulsed-laser-induced dewetting: Competing liquid phase instability and transport mechanisms. *Langmuir* **2010**, *26*, 11972−11979.
(35) González, A. G.; Diez, J. A.; Kondic, L. Stability of a liquid ring on a substrate. Submitted to *J. Fluid Mech.*
(36) Daw, M. S.; Baskes, M. I. Embedded-atom method: Derivation and application to impurities, surfaces, and other defects in metals. *Phys. Rev. B* **1984**, *29*, 6443−6453.
(37) Stuart, S. J.; Tutein, A. B.; Harrison, J. A. A reactive potential for hydrocarbons with intermolecular interactions. *J. Chem. Phys.* **2000**, *112*, 6472−6486.
(38) Frenkel, D.; Smit, B. *Understanding Molecular Simulation: From Algorithms to Applications*; Academic Press: San Diego, 2002.
(39) Naidich, Y. V.; Kolesnichenko, G. A. A study of wetting of diamond and graphite by fused metals and alloys VII. The effect of vanadium, niobium, manganese, molybdenum, and tungsten on wetting of graphite by copper-based alloys. *Powder Metall. Met. Ceram.* **1968**, *3*, 563−565.
(40) Jones, R. O.; Gunnarsson, O. The density functional formalism, its applications and prospects. *Rev. Mod. Phys.* **1989**, *61*, 689−746.
(41) Vanin, M.; Mortensen, J. J.; Kelkkanen, A. K.; Garcia-Lastra, J. M.; Thygesen, K. S.; Jacobsen, K. W. Graphene on metals: A van derWaals density functional study. *Phys. Rev. B* **2010**, *81*, 081408.
(42) Plimpton, S. Fast parallel algorithms for short-range molecular dynamics. *J. Comput. Phys.* **1995**, *117*, 1−19.
(43) Hocking, L. M. Spreading and instability of a viscous fluid sheet. *J. Fluid Mech.* **1990**, *221*, 373−392.
(44) Hocking, L. M. Stability of a ridge of fluid. *J. Fluid. Mech.* **1993**, *247*, 157−177.
(45) Israelachvili, J. N. *Intermolecular and Surface Forces*, Second ed.; Academic Press: New York, 1992.
(46) Butt, H.-J.; Kappl, M. *Surface and Interfacial Forces*; Wiley-VCH Verlag: Weinheim, 2010.
(47) Lin, T.-S.; Kondic, L.; Filippov, A. Thin films flowing down inverted substrates: Three-dimensional flow. *Phys. Fluids* **2012**, *24*, 022105.
(48) Andrieu, C.; Sykes, C.; Brochard, F. Dynamics of fast dewetting on model solid substrates. *J. Adhes.* **1996**, *58*, 15−24.
(49) Fetzer, R.; Münch, A.; Wagner, B.; Rauscher, M.; Jacobs, K. Quantifying hydrodynamic slip: A comprehensive analysis of dewetting profiles. *Langmuir* **2007**, *23*, 10559−10566.
(50) McGraw, J. D.; Li, J.; Tran, D. L.; Shia, A.-C.; Dalnoki-Veress, K. Plateau-Rayleigh instability in a torus: formation and breakup of a polymer ring. *Soft Matter* **2010**, *6*, 1258−1262.